Journal of Nuclear Materials 432 (2013) 61–66

Contents lists available at SciVerse ScienceDirect

Journal of Nuclear Materials

journal homepage: www.elsevier.com/locate/jnucmat

Interatomic potentials for simulation of He bubble formation in W

N. Juslin *, B.D. Wirth

Department of Nuclear Engineering, 315 Pasqua Engineering Building, University of Tennessee, Knoxville, TN 37996-2300, USA

ARTICLE INFO

Article history:
Received 5 April 2012
Accepted 6 July 2012
Available online 3 August 2012

ABSTRACT

A new interatomic pair potential for W–He is described, which includes a short range modification to the Ackland–Thetford tungsten potential. Molecular dynamics simulations using these potentials accurately reproduce *ab initio* results of the formation energies and ground state positions of He point defects and self interstitial atoms in W. Simulations of larger He–vacancy clusters with up to 20 vacancies and 120 He atoms show strong binding of both He and vacancies to He–vacancy clusters for all cluster sizes. For small clusters, the qualitative agreement with *ab initio* results is good, although the vacancy binding energy is overestimated by the interatomic potential.

1. Introduction

Tungsten is a candidate divertor material in fusion reactors, due to its thermal and mechanical properties, such as high melting temperature and thermal conductivity, and low sputtering [1,2]. Low energy (1–100 eV) helium implanted from the fusion plasma, as well as He created in transmutation reactions due to high energy neutron bombardment, will affect the divertor material properties through the formation of gas bubbles and blistering [3]. The extremely low solubility of He in W provides the driving force for He to cluster with itself and other defects and leads to an accumulation of He-defect clusters and bubble formation. Relatively recently it was discovered that during the exposure of a tungsten surface to low energy mixed H/He plasmas at temperatures between about 1000–2000 K, long, low density tendrils are formed [4,5]. The hypothesis is that they are built up around He bubbles, though the mechanism and temperature dependence is still not well understood. How this extreme surface modification affects surface properties and erosion in a real divertor needs to be studied both experimentally and through modeling.

The initial stages of He bubble formation, structure and energetics of smaller bubbles, as well as surface and bulk diffusion mechanisms are well suited for investigation using atomistic molecular dynamics (MD) simulations. MD simulation results can also serve as an important input for Monte Carlo (MC) or cluster dynamics simulations on longer length and time scales. Atomistic simulations require interatomic potentials to calculate the potential energies and forces between atoms. These potentials are usually based on a functional form and fit to experimental and/or *ab initio* results for properties relevant to the desired simulation system. A good potential should be transferable, i.e. be able to describe properties it was not fit to, but all potentials are approximations and compromises have to be made.

For tungsten there are more than 20 different potentials published in the literature, mainly of the Finnis–Sinclair (FS) [6] and embedded atom model (EAM) [7] types, and various modified EAM (MEAM) [8] and bond–order potential (BOP) [9,10] schemes. Most of these are of relatively similar overall quality, each with its own problems, and there is not a single potential which could be clearly identified as the best for all applications. One of the most commonly used potentials is the Ackland–Thetford (AT) modification to the [11] Finnis–Sinclair tungsten potential [6]. This potential is fit to, and generally reproduces, bulk properties. The potential does not, however, describe the Coulombic repulsion at short distances well. Compared to current density functional theory (DFT) calculations [12–14], the interstitial formation energy is also a bit low. Previous modifications of the short range potential have generally been performed at distances on the order of 1–2 Å, which is too short to affect any but high energy phenomena, leaving the interstitials unaffected [15].

There are two commonly used W–He pair potentials. The Wilson potential from 1972 [16] and the potential by Henriksson from 2004 [17]. Neither is published in full analytical form. When the Wilson potential was developed, there was relatively little information available for He defects in W. Its description of He interstitial and substitutional atoms is reasonable, but when compared with *ab initio* results [13] both the ground state position and formation energy do not agree. The potential by Henriksson was developed with a focus on He interstitials, but was fit to modeling data which is in poor agreement with more recent DFT calculations.

In this paper, a new pair potential for W–He is presented, which reproduces simple defect energetics and structures in excellent agreement with DFT results and serves as a good tool for further studies of larger He bubbles. We also introduce a new short range

* Corresponding author. Tel.: +1 865 974 2525; fax: +1 865 974 0668.
E-mail address: njuslin@gmail.com (N. Juslin).

0022-3115/$ - see front matter © 2012 Elsevier B.V. All rights reserved.
http://dx.doi.org/10.1016/j.jnucmat.2012.07.023

modification of the Ackland–Thetford tungsten potential, which in addition to hardening the potential at distances only found in non-equilibrium situations also improves the potential at distances of relevance to self-interstitial configurations. These potentials are applied to study He–vacancy clusters with up to 20 vacancies and 120 He.

2. Methods

2.1. Potentials

The functional formalism chosen for the W–He potential is the same which was recently successfully applied to the Fe–He [18] and Cr–He [19] systems. As the functional form is unable to describe the strong repulsion at very short distances (less than 1 Å), the potential was joined with the Ziegler–Biersack–Littmark (ZBL) potential [20] for short range interactions through a polynomial function, as is commonly done for interatomic potentials. The potential is given by

$$f(r_{ij}) = \begin{cases} ZBL, & r_{ij} \leqslant r_1, \\ p_5 r_{ij}^5 + p_4 r_{ij}^4 + p_3 r_{ij}^3 + p_2 r_{ij}^2 + p_1 r_{ij} + p_0, & r_1 \leqslant r_{ij} \leqslant r_2, \\ \left(a + \frac{b}{r_{ij}}\right) e^{-c r_{ij}} f_c(r_{ij}), & r_{ij} \geqslant r_2, \end{cases} \tag{1}$$

where the cut-off function f_c is given by

$$f_c(r_{ij}) = \begin{cases} 1, & r_{ij} \leqslant r_c - r_d, \\ \frac{1}{2}\left(1 - \sin\frac{\pi(r_{ij} - r_c)}{2r_d}\right), & |r_c - r_{ij}| \leqslant r_d, \\ 0, & r_{ij} \geqslant r_c + r_d, \end{cases} \tag{2}$$

The cut-off is a function that goes smoothly from 1 to 0. This type of cut-off has previously been used in e.g. Tersoff type potentials [21]. The parameters for the potential are provided in Table 1 and a comparison with the Wilson and Henriksson potentials is shown in Fig. 1.

For the short range modification of the Ackland–Thetford tungsten potential, the ZBL potential was used. The pair potential part of the AT EAM potential was fit to ZBL, while the embedding part was left unchanged. In order to obtain a better fit to the AT potential at the desired joining distance, the ZBL potential was reduced by 10 eV. This procedure retains the forces between atoms for the ZBL part, but impacts the joining polynomial between the ZBL potential and the FS potential. A further joining to the normal ZBL could of course be made at even shorter distances, but a 10 eV difference in potential energy at short ranges is of little consequence in simulations, as the potential energy is hundreds or thousands of eV at the ranges where the ZBL potential can be considered valid. A fifth order polynomial was chosen to join the short range and equilibrium range parts of the potential at a distance longer than conventionally used for short range modification of potentials. This was done in order to affect the potential at interstitial distances and improve the formation energies of self interstitials as compared to DFT values. The distance was, however, shorter than the nearest neighbor distance to retain the good bulk properties of the AT potential. The modified part of the potential is

Table 1
Parameters for the new W–He potential. The units are combinations of eV and Å to give Eq. (1) units of eV.

a	−17.68	r_1	1.08	p_0	9.66233069e+02	p_3	−1.59156990e+03
b	66.92	r_2	2.08	p_1	−2.58889382e+03	p_4	4.46397058e+02
c	1.354	r_c	2.858	p_2	2.85120696e+03	p_5	−5.00623967e+01
		r_d	0.306				

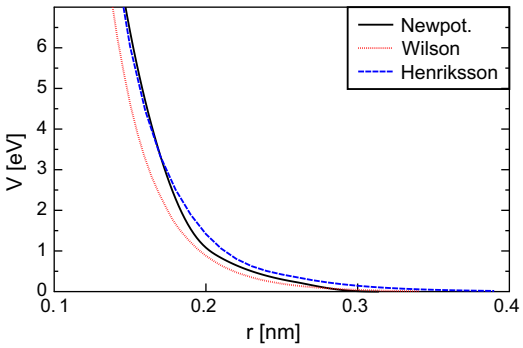

Fig. 1. The new W–He pair potential compared to the potentials by Wilson and Henriksson.

given in Eq. (3) (for the full potentials, see Ref. [11]), the parameters in Table 2 and a visual representation is shown in Fig. 2. As the joining is done at 2.6 Å and the AT potential only differs from the original Finnis–Sinclair (FS) potential below 2.734 Å there is only a small difference between the AT and FS potentials at this distance.

$$V(r_{ij}) = \begin{cases} ZBL - 10eV, & r_{ij} \leqslant r_1 \\ a_5 r_{ij}^5 + a_4 r_{ij}^4 + a_3 r_{ij}^3 + a_2 r_{ij}^2 + a_1 r_{ij} + a_0, & r_1 \leqslant r_{ij} \leqslant r_2, \\ V_{AT} pot. & r_{ij} \geqslant r_2, \end{cases} \tag{3}$$

The tungsten potentials by Derlet–Dudarev et al. (DD) [12] and Juslin–Erhart et al. (JE) [9] were also used for comparison for He interstitials. While the W–He potential was fit to work together with the Ackland–Thetford potential (the modification presented above does not affect the properties the W–He potential was fit to), it can be expected to work well together with other tungsten potentials with similar elastic and defect properties. For He–He, the Beck potential [22] was used, with the short range fit by Morishita [23], which has not been published in full form and is a smooth fit to ZBL below 1 Å.

2.2. MD/MS simulation approach

The MD simulations were performed using the codes PARCAS [24] and LAMMPS [25]. Unless otherwise specified, the simulation cell consisted of a $10 \times 10 \times 10$ body-centered cubic (BCC) lattice of 2000 tungsten atoms, plus the desired defects and helium atoms. Larger simulation cells were tested to ensure that the defect properties did not measurably change. Periodic boundaries were applied in all simulations. To find meta-stable atomic positions, the defects were placed in the corresponding positions and then the system was carefully relaxed to keep the defects from jumping to the ground state position. To ensure the correct ground state, annealing at several different temperatures and rates was performed. The Berendsen temperature and pressure controls were used [26]. The defects were simulated at constant volume.

The formation energy of a defect is calculated as

$$E_f = E_{def} - E_{ref} \cdot (N - m_{\mathrm{vac}})/N + E_{ref,\mathrm{He}} \cdot n_{\mathrm{He}}, \tag{4}$$

where E_{def} is the total energy of the system including the defect, E_{ref} is the energy of the pure tungsten matrix and N is the number of atoms in the pure simulation box. The reference energy used for He, $E_{ref,\mathrm{He}}$, is the cohesive energy of close packed helium, which is very low at −0.0054 eV/atom for the Beck He–He potential.

There are several ways to define the threshold displacement energy, as was thoroughly discussed by Nordlund et al. [27]. The same method was used in this work and will only be briefly re-

Table 2
Parameters for the joining function used to modify the short range order of the pair potential part of the Ackland–Thetford EAM type W–W potential. The units are combinations of eV and Å to give Eq. (3) units of eV.

r_1	1.39139856	a_0	6.02476984e+03	a_2	1.14668996e+04	a_4	1.09903719e+03
r_2	2.60079984	a_1	−1.31022346e+04	a_3	−5.02451407e+03	a_5	−9.58391332e+01

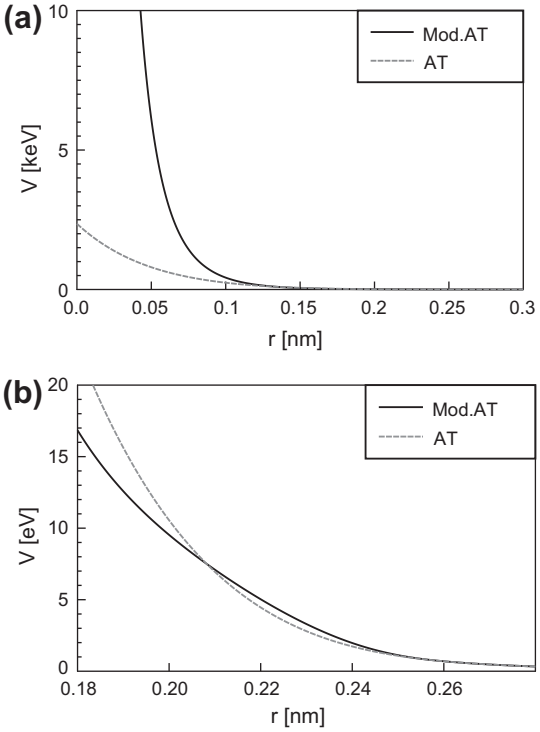

Fig. 2. The modified pair potential part of the Ackland–Thetford tungsten potential compared to the original. (a) Shows how much softer the original AT is compared to the ZBL at less than about 1.4 Å, while (b) shows a closer view of the distances relevant to interstitial properties.

viewed. The crystal directions include a 20° angle smearing to reflect experimental uncertainties. The simulation box was $12 \times 12 \times 16$ to avoid channeling across periodic boundaries in the $\langle 1\,1\,1 \rangle$ direction. In tungsten the experiments are done at low temperatures to avoid recovery of the defect [28]. The system was relaxed to temperatures of 4 K and 10 K, after which a random atom was given a recoil energy in a random direction in increments of 2 eV until a stable Frenkel pair was produced. This process was repeated until sufficient statistics were obtained.

In order to obtain the melting temperature, a two phase system was used. Solid and liquid phases at the same temperatures were joined and the motion of interface region was monitored. If the temperature is above the melting temperature, the interface moves into the solid region as melting occurs, and vice versa with crystallization.

Binding energies of a He atom or a vacancy to a cluster were calculated using:

$$E_b(A_1, A_2) = E(A_1) + E(A_2) - E(A_1 + A_2) - E_{ref}, \quad (5)$$

where A_1 and A_2 are different defects, in this case a He atom or vacancy and a HeV cluster, and $A_1 + A_2$ is the combined defect.

To get the energy and structure of a He_nV_m cluster, first a vacancy cluster with m vacancies was produced by relaxing a $m - 1$ cluster to 0 K and removing the tungsten atom with the highest potential energy. Then n He atoms where placed in random positions inside the void. This system was heated up to between 300 and 900 K and quenched back to 0 K to find the ground state structure of the HeV cluster. For large clusters and those containing high He/vac ratios, substantial stresses exist within the tungsten matrix, and thus it is hard to be certain that the actual ground state has been found. Therefore the cluster structure should probably be considered a meta-stable state close to the ground state. Different starting conditions and annealing schemes, as well as repeated annealing runs, were used to ensure that the results are close to the ground state.

3. Results and discussion

3.1. W–W

The modified Ackland–Thetford potential is identical to the original potential for structures where the tungsten atoms are not closer than $r_1 = 2.6$ Å, which is below the nearest neighbor distance $r_0 = \frac{\sqrt{3}}{2}a_0$, or 2.74 Å, for BCC tungsten. Thus most bulk properties are unchanged, while in particular the interstitial properties are improved compared to DFT results, as shown in Table 3. The differences in formation energy between different interstitial positions are almost the same as for the original potential, but the energy of the ground state position is shifted to agree with DFT results.

Another property affected by the potential at this range is the threshold displacement energy. For the original version the average of the threshold displacement energy over all directions, as well as the lowest energy, is high compared to experiments [28]. The modified AT potential improves both the lowest and the average threshold displacement energies as shown in Table 4, though the average is still high. The results are the same at 4 K and 10 K.

Bulk properties such as elastic constants remain the same in good agreement with experimental values [11]. The melting temperature is unchanged with the modified potential. At 4100 ± 50 K it is higher than the experimental value of 3695 K.

3.2. W–He

The W–He potential was fit to produce formation energies of a single interstitial or substitutional He atom in good agreement with DFT results [13], as shown in Table 5. Substitutional He and the interstitial ground state position and energy are reproduced perfectly, while the energy difference between the tetrahedral and octahedral positions is smaller, though still close to the *ab initio* value, 0.15 eV and 0.22 eV with MD and DFT respectively. The He–He binding energy in W is 0.17 eV lower than DFT, but still demonstrates a strong binding interaction. Compared to the old potentials the agreement with DFT results is significantly improved. The W–He potential described here was developed for

Table 3
The formation energy of the 110 and 111 dumbbell and the octahedral self interstitial positions for the new modified Ackland–Thetford potential, compared to the original Ackland–Thetford (AT), as well as DFT results.

	DFT [12]	AT	ATmod
$E_{f,db110}$ (eV)	9.84	9.61	10.16
$E_{f,db111}$ (eV)	9.55	8.88	9.50
$E_{f,octa}$ (eV)	11.7	9.97	10.39

Table 4
Threshold displacement energies for the new modified Ackland–Thetford (ATmod) potential, compared to the normal Ackland–Thetford (AT) potential, as well as experimental results.

T_d (eV)	Expt. [28]	ATmod	AT
Min.	~40–50	48	64
Ave.	~80	128	166

Table 5
A comparison of the new W–He potential (Jus) with the potentials by Wilson (Wil) [16] and Henriksson (Hen) [17], as well as DFT data, for the formation energy of substitutional He and interstitial He in the tetrahedral and octahedral positions, the He–He binding energy and the migration energy between two tetrahedral positions. All values are in eV.

	DFT [13]	Jus	Wil	Hen
$E_{f,subs}$	4.70	4.70	3.63	6.29
$E_{f,tetr}$	6.16	6.16	4.77	8.20
$E_{f,octa}$	6.38	6.31	4.76	7.94
$E_{b,He-He}$	1.03	0.86	0.81	0.82
E_{mig}	0.06	0.21	0.27	0.28

Table 6
A comparison of He defect formation energies for different W potentials. ATmod is the modification of the Ackland–Thetford potential presented in this paper, DD is the Derlet–Dudarev potential [12] and JE is the Juslin–Erhart potential [9]. The formation energies of substitutional He and interstitial He in the tetrahdral and octahedral positions are given in eV. The low substitutional formation energy for JE is due to the low vacancy formation energy with that potential.

	DFT [13]	ATmod	DD	JE
$E_{f,subs}$	4.70	4.70	4.64	2.59
$E_{f,tetr}$	6.16	6.16	6.83	6.21
$E_{f,octa}$	6.38	6.31	7.15	6.59

use with the AT tungsten potential and if used together with other potentials, the results will depend on the W potential, as shown in Table 6. W potentials with similar stiffness and defect properties can, however, be expected to perform well together with the W–He potential.

The migration energy of He in W predicted by this potential is a bit lower than the previous potentials. Experiments put the value between 0.25 and 0.30 eV, while DFT gives 0.06 eV. The DFT result is for the saddle point between two tetrahedral positions. It has been hypothesized that the experimental results are actually for small He clusters of 1–3 atoms, or could involve trapping/de-trapping with some defect. The new potential gives a saddle point energy of 0.21 eV, which falls between the experimental and *ab initio* results. While it would be possible to further adjust the migration barrier while maintaining other properties to a good degree, the present value was considered a good compromise.

3.3. Small HeV clusters

The binding energy of a divacancy in tungsten calculated by DFT is slightly negative [13,29,14], while the MD potentials commonly used for radiation damage simulations give binding energies between 0.35 and 0.6 eV. In the case of the Ackland–Thetford potential the binding energy is 0.43 eV, while according to the DFT data by Becquart et al. [13,30] it is −0.1 eV. The calculations by Becquart et al. will be used for the comparisons in the rest of this section. This difference continues for larger clusters, with MD giving a binding energy 0.5–1.0 eV higher than DFT, as shown in Fig. 3, up to clusters containing eight vacancies, which are the largest available in the DFT literature.

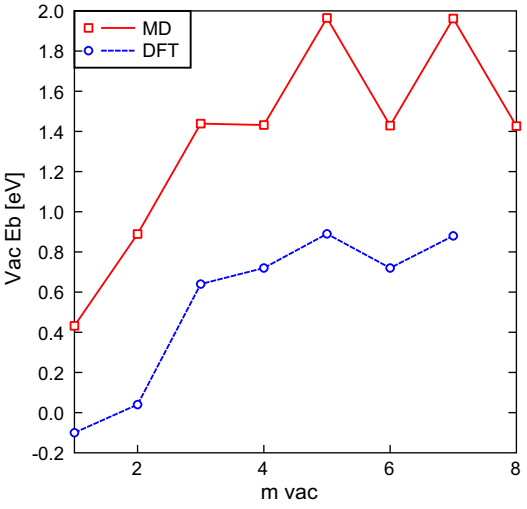

Fig. 3. There are large discrepancies between MD and DFT [30] when it comes to the description of vacancy clusters. The binding energy of a vacancy to a vacancy cluster is significantly higher according to MD than DFT data. Each point represents a V + V_m cluster with a total of m + 1 vacancies.

For small He clusters the MD results are in excellent agreement with DFT results, while there are some discrepancies for small He–vacancy clusters. In the literature, DFT results exist for helium and vacancy binding to clusters with up to four vacancies and a small number of He atoms [29]. A comparison between MD and the available DFT data is shown in Fig. 4 for He binding and Fig. 5 for vacancy binding to a HeV cluster. For pure He clusters, the binding energy in MD is slightly underestimated compared to DFT, but overall the agreement is excellent. With one vacancy these interatomic potentials overestimate the He–V_1 binding energy by 0.5 eV compared to DFT, while the He–He_1V_1 binding energy matches the DFT results. Larger He_nV_1 differ from the DFT values by about 0.5 eV. For larger V_m clusters, the MD results are also consistently about 0.5 eV higher than DFT. While there are some quantitative differences, the qualitative features of the binding energies match very well between MD and DFT.

MD results using this new interatomic potential for He binding to larger clusters with up to 20 vacancies are shown in Fig. 6. For

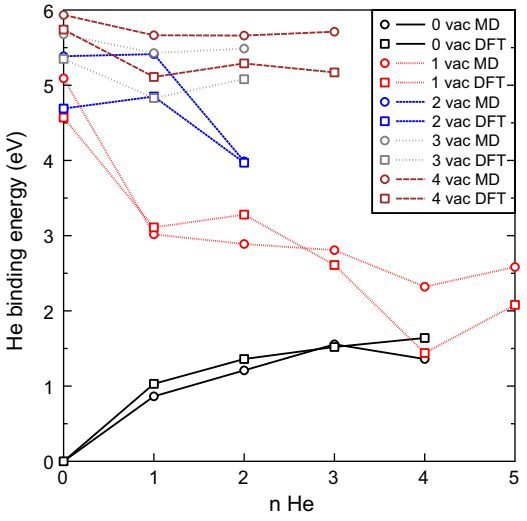

Fig. 4. A comparison of small He–vacancy clusters between MD with the new potentials and DFT [29]. The binding energy is given as a function of the number of He in the cluster for different vacancy cluster sizes. Each point represents a He + He_nV_m cluster with a total of n + 1 He atoms.

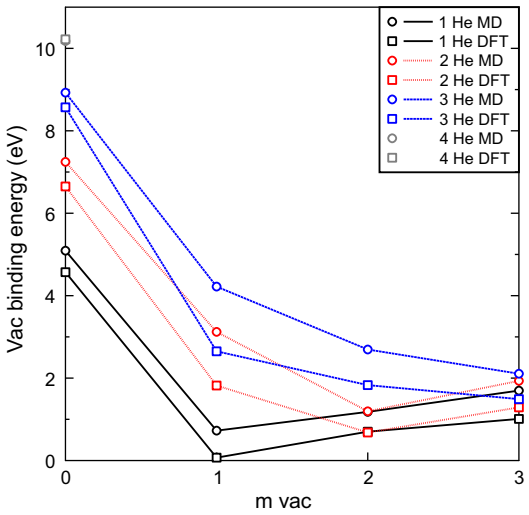

Fig. 5. A comparison between DFT [29] and MD of the binding energy of a vacancy to a HeV cluster as a function of number of vacancies. Each point represents a V + He_nV_m cluster with a total of $m + 1$ vacancies.

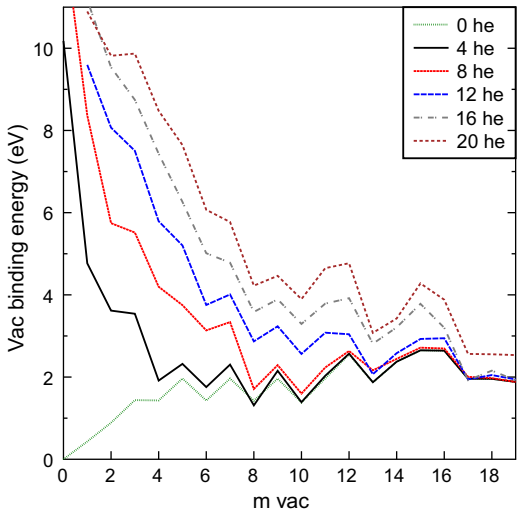

Fig. 7. MD results for the binding energy of a vacancy to a HeV cluster as a function of number of vacancies. Each point represents a V + He_nV_m cluster with a total of $m + 1$ vacancies.

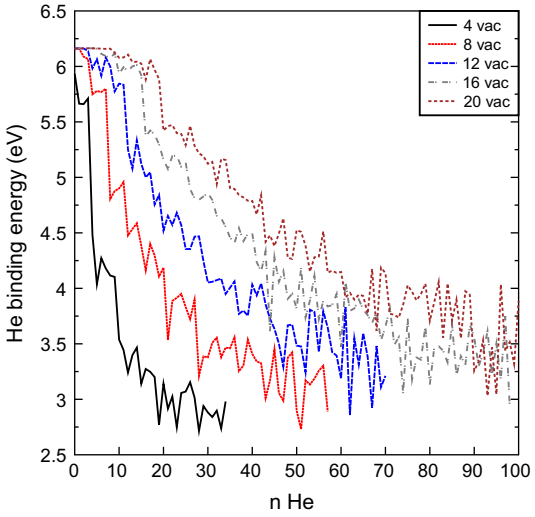

Fig. 6. MD results for He–vacancy clusters of up to 20 vacancies as a function of number of He atoms. Each point represents a He + He_nV_m cluster with a total of $n + 1$ He atoms.

clarity, only vacancy clusters of size 4, 8, 12, 16 and 20 are shown, but the trend is the same for all clusters. Up to $(m_{vac} - 1)$ He, a He atom is strongly bound to the cluster, with a binding energy of around 6 eV, which is close to the formation energy of an interstitial He. At this point there is less volume available for the additional He atom and the He atoms interact more strongly with other He and surrounding tungsten atoms. The binding energy eventually decreases to values around 3–3.5 eV with increasing He content, until the cluster pressure becomes too large and a W interstitial is ejected to provide more volume to release gas pressure. A He atom is strongly bound with a binding energy of at least a couple of eV to a HeV cluster of any size.

The binding energy of a vacancy to larger clusters is presented in Fig. 7. A vacancy is strongly bound to a cluster with a high He/vac ratio and then drops towards the binding energy of a vacancy to a pure vacancy cluster at about 2 eV as the He/vac ratio approaches 1.

While the binding energies for both a He atom and a vacancy to a cluster follow clear trends, there are fluctuations which can be seen as a jagged line in the figures, changing the energy by up to 1 eV with just 1 added defect. This can likely be attributed to more symmetric and energetically favorable structures for certain numbers of vacancies and helium, but could also indicate the possibility of meta-stable states that are not close enough to the ground state.

4. Conclusions

A new potential for W–He was developed. Compared with recent DFT results, the potential performs very well for single He interstitials and small defect clusters, and offers a significant improvement over older potentials. A new short range modification of the Ackland–Thetford W–W potential was also developed, which provides the needed high energy at very short distances, as well as a small modification at interstitial distances. These modifications slightly improve the formation energies of the ground state position compared to DFT. While these new potentials improve the description of He defects and self interstitial atoms in W, in particular the poor agreement with DFT for the divacancy binding energy will require further work on tungsten potentials.

The new potentials were applied to study the structure and energetics of He–vacancy clusters with up to 20 vacancies. For small clusters of up to four vacancies, DFT values are available in the literature for comparison. Overall the energetics and trends when adding He or vacancies are in reasonable agreement between DFT and MD, though the binding energy values vary by about 1 eV.

Both He and vacancy binding energy to a cluster exhibit important trends as a function of cluster size. Except for the smallest clusters with 1–3 vacancies, the He binding energy is around 6 eV, close to the formation energy of a He interstitial, until the total number of He in the cluster is equal to the number of vacancies. The binding energy then drops quickly for the next one or two He atoms, after which it steadily decreases until the number of He is about four times the number of vacancies, where it stabilizes at around 3–4 eV. The vacancy binding energy is very high for high He/vac ratios and approaches the binding energy of a vacancy to a pure vacancy cluster as the ratio goes towards and below about one He per vacancy.

The trends of binding energies of small He–vacancy clusters provide improved understanding of He bubble formation, and are of use for studying larger clusters. This data, and the potentials described here will also be of use for studying how other defects such

as hydrogen, dislocations, grain boundaries and surfaces interact with He–defect clusters. Binding energies from MD also serve as an important input for longer and larger scale simulations.

Acknowledgments

The authors thank the other members of the Plasma Surface Interactions (PSI) Science Center at the Massachusetts Institute of Technology and University of California, San Diego for collaborative discussions about this work. This work has been supported as part of the PSI Science Center by the US Department of Energy under award DE-SC00–02060.

References

[1] G. Janeschitz, J. Nucl. Mater. 290 (2001) 1–11.
[2] H. Bolt, V. Barabash, W. Krauss, J. Linke, R. Neu, S. Suzuki, N. Yoshida, A. Team, J. Nucl. Mater. 329 (2004) 66–73.
[3] H. Lee, A. Haasz, J. Davis, R. Macaulay-Newcombe, J. Nucl. Mater. 360 (2) (2007) 196–207.
[4] M. Baldwin, R. Doerner, Nucl. Fusion 48 (2008) 035001.
[5] S. Kajita, W. Sakaguchi, N. Ohno, N. Yoshida, T. Saeki, Nucl. Fusion 49 (2009) 095005.
[6] M.W. Finnish, J.E. Sinclair, Philos. Mag. A 50 (1984) 45.
[7] M.S. Daw, M.I. Baskes, Phys. Rev. B 29 (12) (1984) 6443.
[8] B. Lee, M. Baskes, H. Kim, Y. Cho, Phys. Rev. B 64 (18) (2001) 184102.
[9] N. Juslin, P. Erhart, P. Träskelin, J. Nord, K.O.E. Henriksson, K. Nordlund, E. Salonen, K. Albe, J. Appl. Phys. 98 (2005) 123520.
[10] M. Mrovec, R. Gröger, A. Bailey, D. Nguyen-Manh, C. Elsässer, V. Vitek, Phys. Rev. B 75 (10) (2007) 104119.
[11] G.J. Ackland, R. Thetford, Philos. Mag. A 56 (1) (1987) 15.
[12] P. Derlet, D. Nguyen-Manh, S. Dudarev, Phys. Rev. B 76 (5) (2007) 054107.
[13] C. Becquart, C. Domain, Nucl. Instrum. Methods Phys. Res. B 255 (1) (2007) 23–26.
[14] L. Ventelon, F. Willaime, C.-C. Fu, M. Heran, I. Ginoux, J. Nucl. Mater. 425 (1–3) (2012) 16–21.
[15] J. Fikar, R. Schäublin, J. Nucl. Mater. 386 (2009) 97–101.
[16] W.D. Wilson, R.A. Johnson, in: P.C. Gehlen, J.R. Beeler, R.I. Jaffee (Eds.), Interatomic Potentials and Simulation of Lattice Defects, Plenum, New York, 1972, p. 375.
[17] K.O.E. Henriksson, K. Nordlund, J. Keinonen, D. Sundholm, M. Patzschke, Phys. Scripta T108 (2004) 95. S,.
[18] N. Juslin, K. Nordlund, J. Nucl. Mater. 382 (2-3) (2008) 143–146.
[19] D. Terentyev, N. Juslin, K. Nordlund, N. Sandberg, J. Appl. Phys. 105 (10) (2009) 103509.
[20] J.F. Ziegler, J.P. Biersack, U. Littmark, The Stopping and Range of Ions in Matter, Pergamon, New York, 1985.
[21] J. Tersoff, Phys. Rev. Lett. 56 (1986) 632.
[22] D.E. Beck, Mol. Phys. 14 (1968) 311.
[23] K. Morishita, R. Sugano, B. Wirth, T. Diaz de La Rubia, Nucl. Instrum. Methods Phys. Res. B 202 (2003) 76–81.
[24] Parcas computer code, K. Nordlund, private communication. The Main Principles of the Molecular Dynamics Algorithms are Presented in [31,32]. The Adaptive Time Step and Electronic Stopping Algorithms are the Same as in [33].
[25] S. Plimpton, J. Comput. Phys. 117 (1995) 1–19.
[26] H.J.C. Berendsen, J.P.M. Postma, W.F. Gunsteren, A.D. Nola, J.R. Haak, J. Chem. Phys. 81 (1984) 3684.
[27] K. Nordlund, J. Wallenius, L. Malerba, Nucl. Instrum. Meth. Phys. Res. B 246 (2) (2005) 322–332.
[28] F. Maury, M. Biget, P. Vajda, A. Lucasson, P. Lucasson, Radiat. Eff. 38 (1-2) (1978) 53–65.
[29] C. Becquart, C. Domain, J. Nucl. Mater. 385 (2) (2009) 223–227.
[30] C. Becquart, C. Domain, U. Sarkar, A. DeBacker, M. Hou, J. Nucl. Mater. 403 (1-3) (2010) 75–88.
[31] K. Nordlund, M. Ghaly, R.S. Averback, M. Caturla, T. Diaz de la Rubia, J. Tarus, Phys. Rev. B 57 (13) (1998) 75567570.
[32] M. Ghaly, K. Nordlund, R.S. Averback, Philos. Mag. A 79 (4) (1999) 795.
[33] K. Nordlund, Comput. Mater. Sci. 3 (1995) 448.